

Numerical Heat Transfer, Part B: Fundamentals



ISSN: 1040-7790 (Print) 1521-0626 (Online) Journal homepage: http://www.tandfonline.com/loi/unhb20

A Coupled Incompressible Flow Solver on Structured Grids

M. Darwish, I. Sraj & F. Moukalled

To cite this article: M. Darwish , I. Sraj & F. Moukalled (2007) A Coupled Incompressible Flow Solver on Structured Grids, Numerical Heat Transfer, Part B: Fundamentals, 52:4, 353-371, DOI: 10.1080/10407790701372785

To link to this article: http://dx.doi.org/10.1080/10407790701372785

	Published online: 21 Aug 2007.
	Submit your article to this journal $oldsymbol{G}$
ılıl	Article views: 218
a a	View related articles 🗗
4	Citing articles: 19 View citing articles 🗹

Full Terms & Conditions of access and use can be found at http://www.tandfonline.com/action/journalInformation?journalCode=unhb20

Copyright © Taylor & Francis Group, LLC ISSN: 1040-7790 print/1521-0626 online

DOI: 10.1080/10407790701372785



A COUPLED INCOMPRESSIBLE FLOW SOLVER ON STRUCTURED GRIDS

M. Darwish, I. Sraj, and F. Moukalled

Department of Mechanical Engineering, American University of Beirut, Riad El Solh, Beirut, Lebanon

This article deals with the formulation, implementation, and testing of a fully coupled velocity-pressure algorithm for the solution of laminar incompressible flow problems. The tight velocity-pressure coupling is developed within the context of a collocated structured grid, and the systems of equations involving velocity and pressure are solved simultaneously. The pressure and momentum equations are derived in a way similar to a segregated SIM-PLE algorithm [1], yielding an extended set of diagonally dominant equations. An algebraic multigrid solver is used to accelerate the solution of the extended system of equations. The performance of the newly developed coupled algorithm is evaluated by solving three test problems showing the effects of grid size, mesh skewness, large pressure gradients, and large source terms on the convergence behavior. Results are presented in the form of convergence history plots and tabulated values of the maximum number of required iterations, the total CPU time, and the CPU time per control volume. This latter performance indicator is shown to be nearly independent of the grid size.

INTRODUCTION

In the numerical solution of fluid flow problems, the discretized Navier-Stokes equations can be solved following either a segregated or a coupled approach. In the segregated approach, the systems of equations for all variables are solved sequentially using fixed, best-estimate values of other dependent variables. This is in contrast to the coupled approach, in which the discretized equations of all variables are solved as one system. Although the coupled-versus-segregated issue is not related directly to the velocity–pressure algorithm, it has traditionally been the case that pressure-based methods, which are the subject of this work, follow a segregated approach, whereas density-based algorithms follow a coupled approach. This situation owes more to the development history of the pressure-based algorithms rather than to any algorithmic limitation.

The segregated pressure-based approach gained popularity in the early 1970s through the development of the SIMPLE algorithm (Semi-Implicit Method for

Received 15 January 2007; accepted 7 March 2007.

Financial support provided by the University Research Board of the American University of Beirut through Grant 14886073129 is gratefully acknowledged.

Address correspondence to F. Moukalled, Department of Mechanical Engineering, American University of Beirut, P.O.Box 11-0236, Riad El Solh, Beirut 1107 2020, Lebanon. E-mail: memouk@aub.edu.lb

		NOMENCLATURE							
$a_P^{\phi}, a_F^{\phi} \dots$ coefficients in the discretized equation for ϕ b_P^{ϕ} source term in the discretized equation for ϕ d_{PF} vector joining the grid points P and F \mathbf{D}_P matrix \mathbf{D} operator g geometric interpolation factor $H[\phi]$ H operator $\mathbf{H}[v]$ vector form of the H operator \dot{m}_f mass flow rate at control-volume face f p pressure P main grid point Q general source term \mathbf{S} surface vector u, v velocity components in x and y directions, respectively \mathbf{v} velocity vector Γ diffusion coefficient dynamic viscosity	Ω _P ρ Subscript e E f F nb NB P x, y Superscri p u v x	refers to the east control-volume face refers to the east grid point refers to control-volume face refers to the <i>F</i> grid point refers to values at the faces obtained by interpolation between <i>P</i> and its neighbors refers to the neighbors of the <i>P</i> grid point refers to the <i>P</i> grid point refers to and <i>y</i> directions							

Pressure Linked Equations) [1] for the solution of incompressible flows. The computational fluid dynamics (CFD) community widely adopted the SIMPLE algorithm, which led to the development of a family of SIMPLE-like algorithms [2–4]. The work of Rhie and Chow [5] and Hsu [6] further advanced the application area of the SIMPLE-like algorithms by enabling the use of a collocated variable arrangement [7] and thereby setting the groundwork for a geometric flexibility similar to that of the finite-element method (FEM) [8].

The first pressure-based coupled solver was developed prior to the SIMPLE algorithm, by Carretto et al. [9] under the acronym SIVA (SImultaneous Variable Arrangement). However, in spite of its merits, the SIVA algorithm was quickly overshadowed by the SIMPLE algorithm, which combined low memory requirement with coding simplicity, which were the two decisive factors given the state of computer technology at that time. Later work resulted in the development of several pressure-based coupled algorithms, which can be divided into two groups. In the first group, the Navier-Stokes equations are discretized in a straightforward manner, i.e., no pressure equation is introduced. Examples in this group include the symmetric coupled Gauss Seidel (SCGS) algorithm of Vanka [10], the UVP method of Karki and Mongia [11], the method of Braaten [12], and, more recently, the body implicit procedure (BIP) of Mazhar [13]. The absence of a pressure equation in the aforementioned algorithms leads to an ill-conditioned system of equations because of the presence of zeros in the main diagonal of the continuity equation. These zeros are treated either by preconditioning [13, 14] or through the use of a penalty formulation [15], or by an algebraic manipulation as in the work of Zedan and Schneider [16] and Galpin et al. [17]. In all cases, these treatments may give rise to stiff equations.

In the second group, a pressure equation is derived in the same way as in the SIMPLE algorithm, yielding an extended set of diagonally dominant equations. Within this group, two approaches are followed. In the first [18], a pressure equation involving pseudo-velocities, as in the SIMPLER algorithm [3], is used. In the second, a segregated pressure equation is developed without the addition of new variables [19]. Using the control-volume finite-element method (CVFEM), Lonsdale [20] followed the second approach and reported impressive convergence rates and good scaling behavior with dense meshes. However, Lonsdale's algorithm did not prove to be robust [21]. In later work, using the Rhie-Chow interpolation, Webster [21, 22] improved on Lonsdale's work and showed that substantial improvement in convergence and decrease in computational time can be achieved through the use of coupled algorithms.

The work presented in this article can be viewed as a continuation of the work of Webster in the context of the finite-volume method (FVM). The tight velocity—pressure coupling is developed on a collocated structured grid, and the systems of equations involving velocity and pressure are solved simultaneously. Following Lonsdale [20] and Webster [21, 22], an algebraic multigrid solver is used to accelerate the solution of the extended system of equations. The performance of the coupled algorithm is evaluated by solving three test problems showing the effects of grid size, mesh skewness, large pressure gradients, and large source terms on the convergence behavior. The focus of the evaluation is to investigate the scalability of the coupled algorithm with increasing mesh density in terms of the number of iterations and CPU time per grid point.

In the remainder of this article, a brief description of the finite-volume discretization process is given, followed by a short review of the Rhie-Chow interpolation used in this work. The coupled algorithm is presented and its implementation detailed. Finally, a number of problems are solved to illustrate the advantages of the fully coupled strategy.

FINITE-VOLUME DISCRETIZATION

The conservation equations governing steady, laminar, incompressible Newtonian fluid flow are given by

$$\nabla \cdot (\rho \mathbf{v}) = 0 \tag{1}$$

$$\nabla \cdot (\rho \mathbf{v} \mathbf{v}) = \nabla \cdot (\mu \nabla \mathbf{v}) - \nabla \cdot p \mathbf{I} \tag{2}$$

These equations can be expressed in the general form

$$\nabla \cdot (\rho \mathbf{v} \phi) = \nabla \cdot (\Gamma \nabla \phi) + Q \tag{3}$$

where the values of ϕ and Γ differ depending on the equation represented.

In the FVM, the domain is discretized by dividing it into a number of control volumes, each associated with a main grid point placed at its geometric center. The discretization of the governing conservation equations is accomplished by integrating the general transport equation over the control volume displayed in

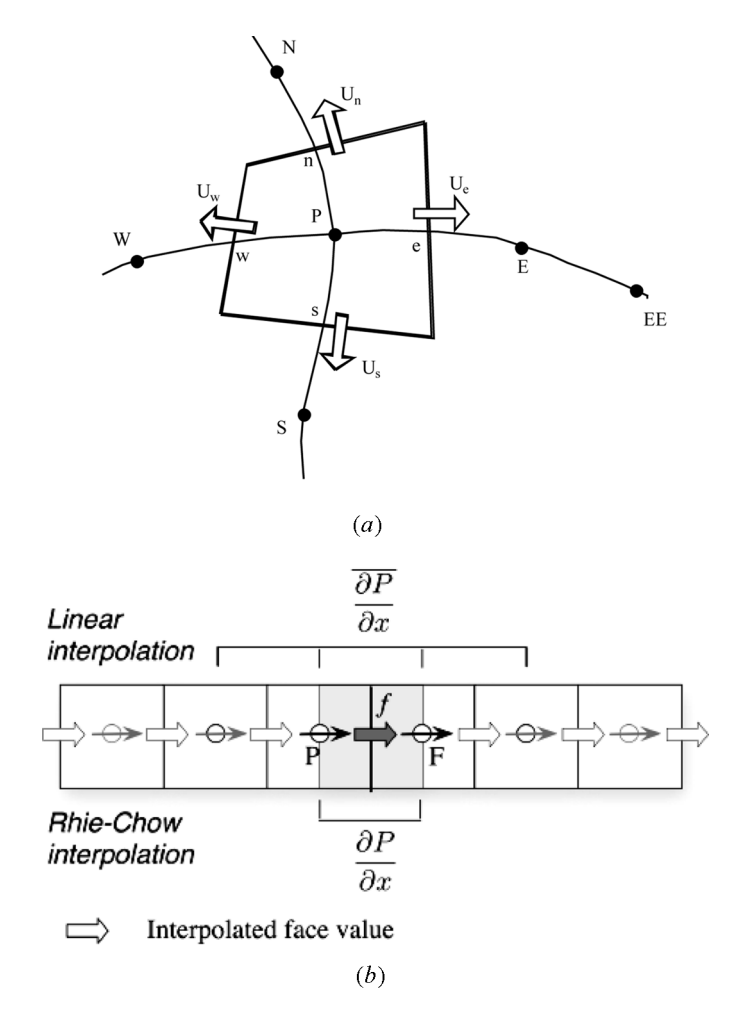


Figure 1. (a) Control volume. (b) Schematic of the Rhie-Chow interpolation.

Figure 1a, to yield

$$\iint_{\Omega} \nabla \cdot (\rho \mathbf{v} \phi) \, d\Omega = \iint_{\Omega} \nabla \cdot (\Gamma \nabla \phi) \, d\Omega + \iint_{\Omega} Q \, d\Omega \tag{4}$$

Using the divergence theorem, the volume integrals in Eq. (4) are transformed into surface integrals as

$$\oint_{\partial\Omega} (\rho \mathbf{v} \phi) \cdot d\mathbf{S} = \oint_{\partial\Omega} (\Gamma \nabla \phi) \cdot d\mathbf{S} + \iint_{\Omega} Q \, d\Omega \tag{5}$$

Then, evaluating these integrals using a second-order integration scheme (trapezoidal rule), Eq. (5) becomes

$$\sum_{f=\text{nb}(P)} (\rho \mathbf{v} \phi - \Gamma \nabla \phi)_f \cdot \mathbf{S}_f = Q_P \Omega_P$$
 (6)

Finally, the equation is transformed into an algebraic equation by expressing the variation in the dependent variable and its derivatives in terms of the grid-point values. The resulting equation, linking the value of the dependent variable at the control-volume center to the neighboring dependent variable values, is written as

$$a_P^{\phi} \phi_P + \sum_{F = \text{NB}(P)} a_F^{\phi} \phi_F = b_P^{\phi} \tag{7}$$

For an upwind (zero-order) profile for convection and a symmetric linear profile for diffusion, the coefficients are given by

$$a_{P}^{\phi} = \sum_{f=\text{nb}(P)} \left\{ \Gamma_{f} \frac{\mathbf{S}_{f} \cdot \mathbf{S}_{f}}{\mathbf{S}_{f} \cdot \mathbf{d}_{PF}} + \left\| \dot{\mathbf{m}}_{f}, 0 \right\| \right\}$$

$$a_{F}^{\phi} = \Gamma_{f} \frac{\mathbf{S}_{f} \cdot \mathbf{S}_{f}}{\mathbf{S}_{f} \cdot \mathbf{d}_{PF}} + \left\| \dot{\mathbf{m}}_{f}, 0 \right\|$$

$$b_{P}^{\phi} = O_{P} \Omega_{P}$$
(8)

where

$$\dot{m}_f = (\rho \mathbf{v})_f \cdot \mathbf{S}_f \tag{9}$$

The above equation could equivalently be written as

$$\phi_P + \frac{\sum\limits_{F = \text{NB}(P)} a_F \phi_F - b_P}{a_P} = 0 \quad \text{or} \quad \phi_P + H_P[\phi] = \mathbf{0}$$
 (10)

For the momentum equation, the pressure gradient term is explicitly displayed as

$$\mathbf{v}_P + \mathbf{H}_P[\mathbf{v}] = -\mathbf{D}_P \nabla p_P \text{ with } \mathbf{D}_P = \begin{bmatrix} d_P^u & 0\\ 0 & d_P^v \end{bmatrix} = \begin{bmatrix} \frac{\Omega_P}{a_P^u} & 0\\ 0 & \frac{\Omega_P}{a_P^v} \end{bmatrix}$$
(11)

For the continuity equation, the following discrete form is used:

$$\sum_{f=\text{nb}(P)} \dot{m}_f = 0 \tag{12}$$

THE RHIE-CHOW INTERPOLATION

The development of the Rhie-Chow interpolation procedure [5] for the calculation of the velocity components at a control-volume face enabled the formulation of the SIMPLE algorithm on collocated grids. In this procedure the interface velocity vector is obtained by constructing a pseudo-momentum equation at the control-volume face from the momentum equations of cells P and F (Figure 1b) straddling the interface. These equations are given by

$$\mathbf{v}_P + \mathbf{H}_P[\mathbf{v}] = -\mathbf{D}_P \nabla p_P$$
 and $\mathbf{v}_F + \mathbf{H}_F[\mathbf{v}] = -\mathbf{D}_F \nabla p_F$ (13)

The pseudo-momentum equation for \mathbf{v}_f should be similar to Eq. (13) and can be written as

$$\mathbf{v}_f + \mathbf{H}_f[\mathbf{v}] = -\mathbf{D}_f \nabla p_f \tag{14}$$

Because on a collocated grid the coefficients of this equation cannot be computed directly, they are approximated by interpolation from the coefficients of the neighboring nodes. Using a simple linear interpolation profile, these coefficients are computed as

$$\begin{cases}
\mathbf{H}_{f}[\mathbf{v}] = g_{f}\mathbf{H}_{P}[\mathbf{v}] + (1 - g_{f})\mathbf{H}_{F}[\mathbf{v}] = \overline{\mathbf{H}_{f}}[\mathbf{v}] \\
\mathbf{D}_{f} = g_{f}\mathbf{D}_{P} + (1 - g_{f})\mathbf{D}_{F} = \overline{\mathbf{D}_{f}}
\end{cases}$$
(15)

where g_f is a geometric interpolation factor ($g_f = 1/2$ for a uniform grid). Using these values for \mathbf{H}_f and \mathbf{D}_f , the pseudo-momentum equation at the control-volume face becomes

$$\mathbf{v}_f + \overline{\mathbf{H}_f}[\mathbf{v}] = -\overline{\mathbf{D}_f} \nabla p_f \tag{16}$$

In terms of velocity and pressure, $\overline{\mathbf{H}_f}[\mathbf{v}]$ can also be expressed as

$$\overline{\mathbf{H}_f}[\mathbf{v}] = g_f[-\mathbf{v}_P - \mathbf{D}_P \nabla p_P] + (1 - g_f)[-\mathbf{v}_F - \mathbf{D}_F \nabla p_F] = -\overline{\mathbf{v}_f} - \overline{\mathbf{D}_f} \overline{\nabla p_f}$$
(17)

Substituting into Eq. (16), the interface velocity vector is obtained as

$$\mathbf{v}_f = \underbrace{\overline{\mathbf{v}_f}}_{\text{average velocity}} - \underbrace{\overline{\mathbf{D}_f}(\nabla p_f - \overline{\nabla p_f})}_{\text{correction term}}$$
(18)

The prominent feature of Eq. (18) is the strong dependence of the face velocity on the pressure of the adjacent cells, which closely resembles the staggered-grid practice [23, 24].

THE COUPLED ALGORITHM

In the coupled approach, the continuity and momentum equations are solved simultaneously to obtain pressure and velocity fields that satisfy them both. Rather than a pressure-correction equation, a pressure equation is derived from the continuity equation. The discretization of the momentum and continuity equations in the coupled approach differs from the segregated approach in few details.

The discretization starts by integrating the momentum equation over the control volume shown in Figure 1 to yield

$$\iint_{\Omega} \nabla \cdot (\rho \mathbf{v} \mathbf{v}) \, d\Omega = \iint_{\Omega} \nabla \cdot (\mu \nabla \mathbf{v}) \, d\Omega - \iint_{\Omega} \nabla \cdot p \mathbf{I} \, d\Omega + \iint_{\Omega} \mathbf{b} \, d\Omega \tag{19}$$

Next, changing the volume integrals of the convection, diffusion, and pressure gradient terms into surface integrals through the use of the divergence theorem results in

$$\oint_{\partial\Omega} (\rho \mathbf{v} \mathbf{v}) \cdot d\mathbf{S} = \oint_{\partial\Omega} (\mu \nabla \mathbf{v}) \cdot d\mathbf{S} - \oint_{\partial\Omega} p \mathbf{I} \cdot d\mathbf{S} + \iint_{\Omega} \mathbf{b} \, d\Omega$$
 (20)

Then, replacing the surface integrals with discrete summations over the faces of the control volume, the following semidiscretized equation is obtained:

$$\sum_{f=\text{nb}(P)} (\rho \mathbf{v} \mathbf{v} - \mu \nabla \mathbf{v})_f \cdot \mathbf{S}_f + \sum_{f=\text{nb}(P)} p_f \mathbf{S}_f = \mathbf{b}_P \Omega_P$$
 (21)

Last, discretizing Eq. (21), as described earlier, and noting that

$$p_f = g_f p_P + (1 - g_f) p_F (22)$$

the final forms of the discretized momentum equations can be written as

$$\begin{cases}
a_{P}^{uu}u_{P} + \underline{a_{P}^{uv}v_{P}} + \underline{a_{P}^{up}p_{P}} + \sum_{F=NB(P)} a_{F}^{uu}u_{F} + \sum_{F=NB(P)} a_{F}^{uv}v_{F} + \sum_{F=NB(P)} a_{F}^{up}v_{F} = b_{P}^{u} \\
a_{P}^{vv}v_{P} + \underline{a_{P}^{vu}u_{P}} + \underline{a_{P}^{vp}p_{P}} + \sum_{F=NB(P)} a_{F}^{vv}v_{F} + \underbrace{\sum_{F=NB(P)} a_{F}^{vu}u_{F}}_{F=NB(P)} + \underbrace{\sum_{F=NB(P)} a_{F}^{vp}p_{F}}_{F=NB(P)} = b_{P}^{v}
\end{cases}$$
(23)

where the coefficients of the pressure terms are given by

$$a_P^{up} = \sum_{f=\text{nb}(P)} g_f S_f^x \qquad a_F^{up} = (1 - g_f) S_f^x$$

$$a_P^{vp} = \sum_{f=\text{nb}(P)} g_f S_f^y \qquad a_F^{vp} = (1 - g_f) S_f^y$$
(24)

and the remaining coefficients are given as in Eq. (8). It should be noted that the single-underlined terms are due to the pressure gradient, which is now implicitly discretized, while the double-underlined terms are present only at the wall boundaries and are due to the way in which the shear stresses at the walls are evaluated.

The semidiscretized form of the continuity equation, obtained following the same procedure as outlined above, is given by

$$\sum_{f=\operatorname{nb}(P)} \rho_f \mathbf{v}_f \cdot \mathbf{S}_f = 0 \tag{25}$$

Using the Rhie-Chow interpolation, the continuity equation becomes

$$\sum_{f=\mathrm{nb}(P)} \rho_f \left[\overline{\mathbf{v}_f} - \overline{\mathbf{D}_f} (\nabla p_f - \overline{\nabla p_f}) \right] \cdot \mathbf{S}_f = 0$$
 (26)

In its expanded form, Eq. (26) is expressed as

$$\sum_{f=\mathrm{nb}(P)} \rho_f(-\overline{\mathbf{D}_f} \nabla p_f) \cdot \mathbf{S}_f + \sum_{f=\mathrm{nb}(P)} \rho_f \overline{\mathbf{v}_f} \cdot \mathbf{S}_f = \sum_{f=\mathrm{nb}(P)} \rho_f(-\overline{\mathbf{D}_f} \overline{\nabla p_f}) \cdot \mathbf{S}_f$$
 (27)

Noting that

$$\overline{\mathbf{v}_f} = g_f \mathbf{v}_P + (1 - g_f) \mathbf{v}_F \tag{28}$$

the final form of the continuity or pressure equation is written as

$$a_{P}^{pp}p_{P} + \underline{a_{P}^{pu}u_{P} + a_{P}^{pv}v_{P}} + \sum_{F = NB(P)} a_{F}^{pp}p_{F} + \sum_{F = NB(P)} a_{F}^{pu}u_{F} + \sum_{F = NB(P)} a_{F}^{pv}v_{F} = b_{P}^{p}$$
 (29)

where the coefficients in the underlined velocity terms are given by

$$d_P^{pu} = \sum_{f=\text{nb}(P)} g_f S_f^x \qquad d_F^{pu} = (1 - g_f) S_f^x$$

$$d_P^{pv} = \sum_{f=\text{nb}(P)} g_f S_f^y \qquad d_F^{pv} = (1 - g_f) S_f^y$$
(30)

and the expressions of the remaining coefficients are the same as their counterparts in the pressure-correction equation of the segregated algorithm [4].

Combining the discretized momentum [Eq. (23)] and continuity [Eq. (29)] equations, the following system of equations, written in matrix form, at every grid point of the domain is obtained:

$$\begin{bmatrix} a_P^{uu} & a_P^{uv} & a_P^{up} \\ a_P^{vu} & a_P^{vv} & a_P^{vp} \\ a_P^{pu} & a_P^{pv} & a_P^{pp} \end{bmatrix} \begin{bmatrix} u_P \\ v_P \\ p_P \end{bmatrix} + \sum_{F = NB(P)} \begin{bmatrix} a_F^{uu} & a_F^{uv} & a_F^{up} \\ a_F^{vu} & a_F^{vv} & a_F^{pp} \\ a_F^{pu} & a_F^{pv} & a_F^{pp} \end{bmatrix} \begin{bmatrix} u_F \\ v_F \\ p_F \end{bmatrix} = \begin{bmatrix} b_P^{u} \\ b_P^{v} \\ b_P^{v} \end{bmatrix}$$
(31)

The collection of all such systems over the domain results in a system of equations whose size depends on the number of grid points used. In matrix form this system is given by

As is evident, the variables in the different equations are treated implicitly. This practice is the cornerstone of the coupled algorithm approach and is the source of the

convergence acceleration. Moreover, no pressure correction is applied to the velocity field, because the system of equations resolves all variables simultaneously.

The overall coupled algorithm can be summarized as follows.

- 1. Start with the *n*th iteration values $(\dot{m}_f^{(n)}, \mathbf{v}^{(n)}, p^{(n)})$. 2. Assemble and solve the momentum and continuity equations for \mathbf{v}^* and p^* .
- 3. Assemble \dot{m}_f^* using the Rhie-Chow interpolation.
- 3. Solve sequentially all other scalar equations.
- 4. Return to the first step and repeat until convergence.

RESULTS AND DISCUSSION

The performance of the coupled algorithm is assessed by presenting solutions to three laminar, incompressible fluid flow problems: (1) flow behind a backwardfacing step, (2) lid-driven flow in a skew cavity, and (3) natural convection in a trapezoidal cavity. For all problems results are generated using six grid sizes with values of 10^4 , 3×10^4 , 5×10^4 , 10^5 , 2×10^5 , and 3×10^5 control volumes. The largest grid used was limited by the computational resources available and not because of any algorithmic limitation. The same initial guess was used for all grid sizes, and computations were stopped when the maximum residual of all variables, defined as

$$\begin{cases} (RES)^{\phi} = \max_{i=1}^{N} \frac{\left| a_{P}^{\phi} \phi_{P} + \sum_{F \in NB(P)} a_{F}^{\phi} \phi_{F} - b_{P}^{\phi} \right|}{a_{FP}^{\phi} \phi_{scale}} \\ \text{where} \\ \phi_{scale} = \max(\phi_{P, \max} - \phi_{P, \min}, \phi_{P, \max}) \quad \phi_{P, \max} = \max_{i=1}^{N} (\phi_{P}) \quad \phi_{P, \min} = \min_{i=1}^{N} (\phi_{P}) \end{cases}$$

$$(33)$$

became smaller than a vanishing quantity ε , which was set at 10^{-5} . All computations were performed on a MacBook Pro computer with a 2.16-GHz Intel Core Duo processor and 2 GB of RAM.

Results for all the grid networks used are presented in the form of convergence history plots with tabulated values of the maximum number of iterations required, the total CPU time, and the CPU time per control volume.

Problem 1: Flow behind a Backward-Facing Step

Separated flows behind steps arise in many practical situations such as in electronic equipment and combustors. Because of its practical importance, this problem has become an important validation test for CFD code developers and is used here to check the effect of a high pressure gradient on the performance of the coupled approach. The geometry of the case considered is illustrated in Figure 2a and consists of a channel with a length $L = 150 \,\mathrm{mm}$ and a height $H = 10 \,\mathrm{mm}$, with a step at the inlet with dimension $S = 4.9 \,\mathrm{mm}$. The problem is solved for a Reynolds number value, based on the hydraulic diameter, of 200.

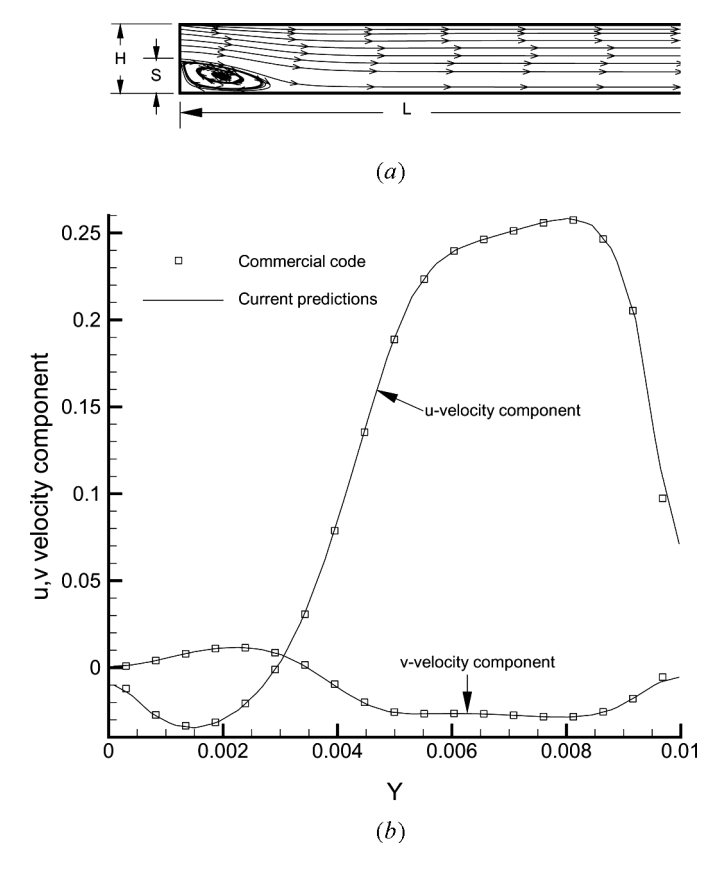


Figure 2. (a) Physical situation and streamlines of the flow behind a backward-facing step. (b) Comparison of predictions obtained with the newly coupled solver against results generated by using a commercial code for the flow behind a backward-facing step.

Results are validated by comparing predictions generated by the coupled approach against those obtained from a commercial segregated CFD code and are presented in Figure 2b. As shown, the u- and v-velocity profiles across the channel at a distance of 4 mm from the inlet (within the recirculation zone) predicted by both methods fall on top of each other, demonstrating the correct implementation of the coupled solver.

A summary of the number of iterations, the CPU time, and CPU time per control volume are presented for all grid sizes in Table 1. As depicted, the number of iterations varies between 18, for a grid size of 10,000 control volumes, and 27, for a grid size of 300,000 control volumes. The CPU time increases from 20.28 s for the case of 10,000 control volumes to 937.53 s for the case of 300,000 control volumes. A more indicative performance parameter is the CPU per control volume, which increases from 0.00203 s to 0.00313 s when the grid size increases from 10,000 to 300,000 control volumes. This represents around a 50% increase in the solution cost per control volume for a 2,900% increase in the mesh size. This performance of the coupled solver is further demonstrated by the residual history plots of the continuity and momentum equations for all grid sizes presented in Figures 3*a*–3*f*.

Size	Iterations	CPU (s)	CPU/CV (s)
10,000	18	20.28	0.00203
30,000	18	59.04	0.00197
50,000	19	97.8	0.00196
100,000	21	238.3	0.00238
200,000	25	491.72	0.00246
300,000	27	937.53	0.00313

Table 1. Number of iterations and computation time required by the coupled solver for the flow behind a backward-facing step

CV, Control volume.

As shown, the convergence paths for all cases are similar, and the convergence rate is nearly independent of the grid size.

Problem 2: Lid-Driven Flow in a Skew Cavity

This problem has also become a standard CFD test case. It is used here to check the performance of the coupled approach in predicting recirculating flows on nonorthogonal grids. A schematic of the physical situation and streamlines are depicted in Figure 4a. Results are presented for a value of Reynolds number (Re = $\rho UL/\mu$, L the cavity height or width and U the velocity of the top horizontal wall) of 1,000. The side walls are skewed at an angle of 60° with respect to the horizontal.

Results are validated by comparing predictions generated by the coupled approach against those obtained from a commercial segregated CFD code and are presented in Figure 4b. As shown, the *u*- and *v*-velocity profiles along the horizontal centerline of the cavity predicted by both methods fall on top of each other, demonstrating again the correct implementation of the coupled solver.

A summary of the number of iterations, the CPU time, and CPU time per control volume are presented for all grid sizes in Table 2. As depicted, the number of iterations varies between 17, for a grid size of 10,000 control volumes, and 20, for a grid size of 300,000 control volumes (with 21 iterations being required for the 200,000 control volumes case). The CPU time increases from 30.08 s for the case of 10,000 control volumes to 1272.14 s for the case of 300,000 control volumes. On the other hand, the CPU per control volume increases from 0.00308 s to 0.00424 s when the grid size increases from 10,000 to 300,000 control volumes (with the value for the 200,000 control volumes being slightly higher at 0.00439 s). This represents around a 38% increase in the solution cost per control volume for a 2,900% increase in the mesh size. This performance of the coupled solver is further demonstrated by the residual history plots of the continuity and momentum equations for all grid sizes presented in Figures 5a-5f. Again, the plots reveal that the convergence paths for all cases are similar and the convergence rate is nearly independent of the grid size.

Problem 3: Buoyancy-Induced Flow in a Trapezoidal Cavity

A schematic of the physical situation under consideration and streamlines are shown in Figure 6a. The cavity is similar to the one analyzed in [25, 26] and has a

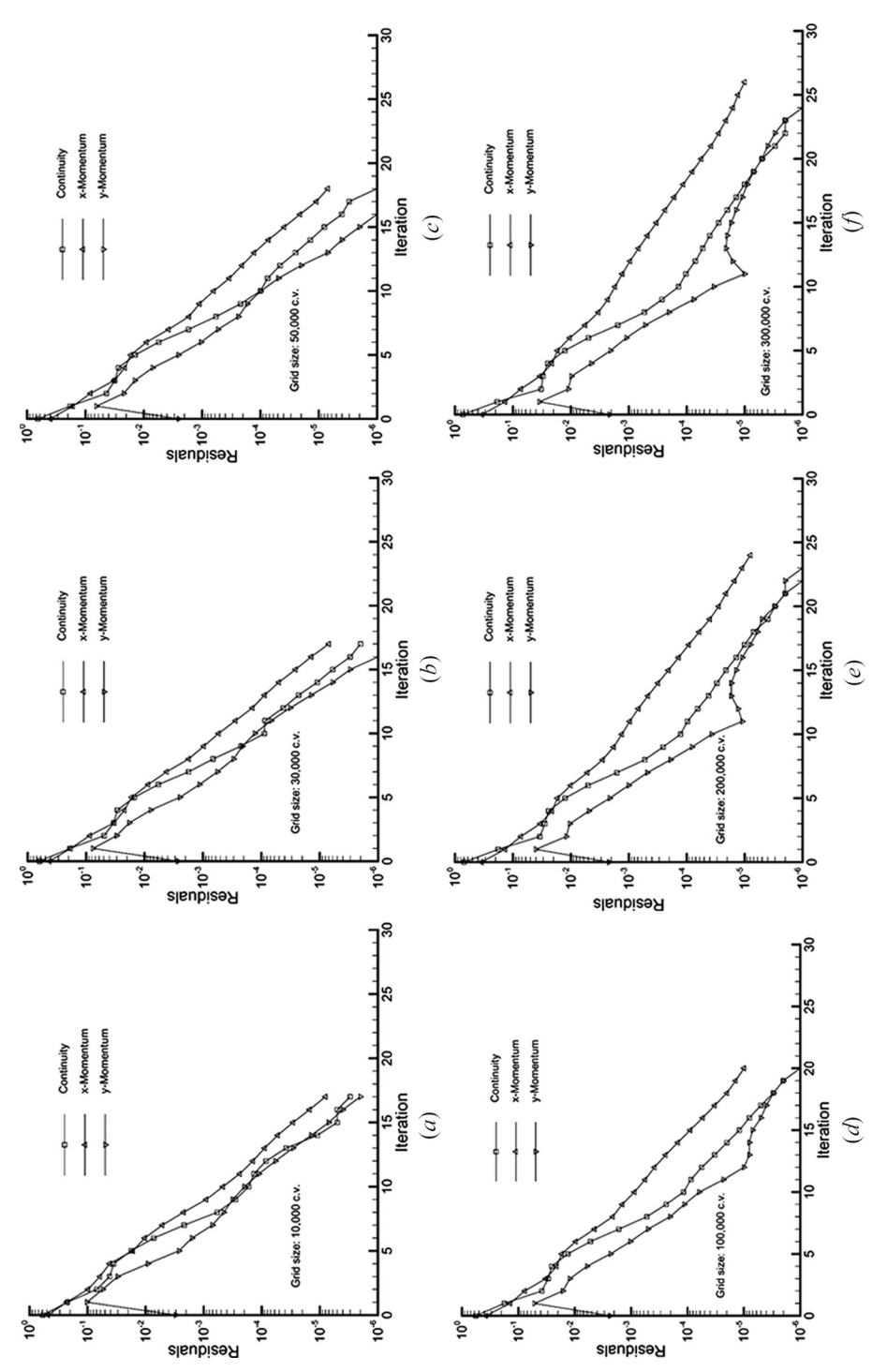


Figure 3. Residual history plots on the various grids for the flow behind a backward-facing step.

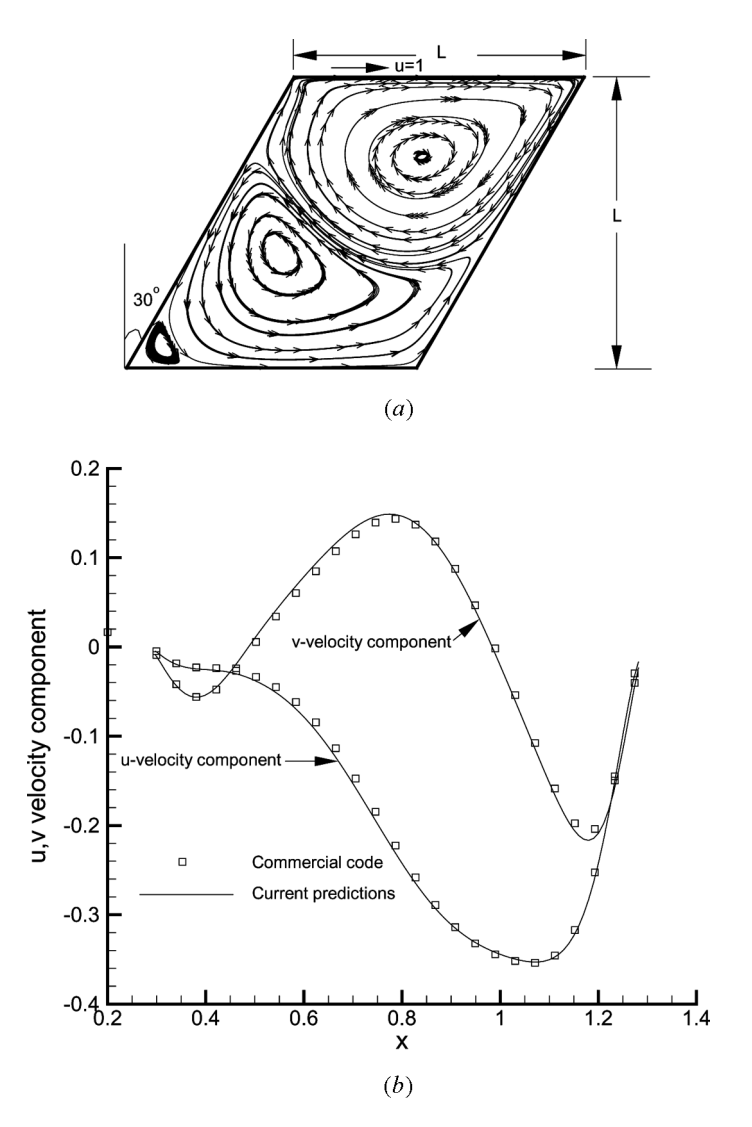


Figure 4. (a) Physical situation and streamlines of the lid-driven flow in a skew cavity. (b) Comparison of predictions obtained with the newly coupled solver against results generated using a commercial code for the lid-driven flow in a skew cavity.

width L that is 4 times the height H of the short vertical wall. The inclination of the top of the cavity is fixed at 15°. The solution for natural convection within the cavity is obtained for the case where the left short vertical wall of the cavity is maintained at the dimensionless uniform hot temperature $\theta_h = 1$ and the right long vertical wall is maintained at the dimensionless uniform cold temperature $\theta_c = 0$. The lower horizontal base and upper inclined plane of the cavity are insulated. The equations governing the flow and heat transfer are those expressing the conservation of mass, momentum, and energy. The flow is assumed to be laminar, steady,

Size	Iterations	CPU (s)	CPU/CV (s)
10,000	17	30.08	0.00308
30,000	17	99.53	0.00332
50,000	18	177.24	0.00354
100,000	20	411.31	0.00411
200,000	21	877.54	0.00439
300,000	20	1272.14	0.00424

Table 2. Number of iterations and computation time required by the coupled solver for the lid-driven flow in a skew cavity

CV. Control volume.

and two-dimensional, with constant fluid properties, except for the induced variations in the body force term. Thus, the physical model requires solving the energy equation in addition to the Navier-Stokes equations while adding the body force term to the *y*-momentum equation (in the direction of gravity). This temperature-dependent body force term is treated as a source term and by adopting a Boussinesq formulation, it is written in a dimensionless form as

$$B_{y} = \frac{\mathrm{Ra}}{\mathrm{Pr}} \,\theta \tag{34}$$

where θ is the dimensionless temperature (as defined in [25, 26]), Ra is the Rayleigh number, and Pr is the Prandtl number. The problem is solved for Ra = 10^5 and Pr = 1. This problem serves as a check on the performance of the new algorithm when sequentially solving the energy equation with the coupled hydrodynamic equations in the presence of a large source term on nonorthogonal grids.

Results are validated by comparing predictions generated by the coupled solver against segregated values reported in [25, 26] and are presented in Figure 6b. As shown, the *u*-velocity and temperature profiles along a vertical line located at the middle of the cavity predicted by both methods fall on top of each other, demonstrating for a third time the correct implementation of the new coupled solver.

A summary of the number of iterations, the CPU time, and the CPU time per control volume are presented for all grid sizes in Table 3. As depicted, the number of iterations varies between 25, for a grid size of 10,000 control volumes, and 22, for a grid size of 300,000 control volumes. The CPU time increases from 44.42 s for the 10,000 control-volumes case to 2020.93 s for the case of 300,000 control volumes. On the other hand, the CPU per control volume increases from 0.0044 s to 0.00674 s when the grid size increases from 10,000 to 300,000 control volumes. This represents around 51% increase in the solution cost per control volume for a 2,900% increase in the mesh size. This performance of the coupled solver is further demonstrated by the residual history plots of the continuity and momentum equations for all grid sizes presented in Figures 7a-7f. Again, the plots reveal that the convergence paths for all cases are similar and the convergence rate is nearly independent of the grid size.

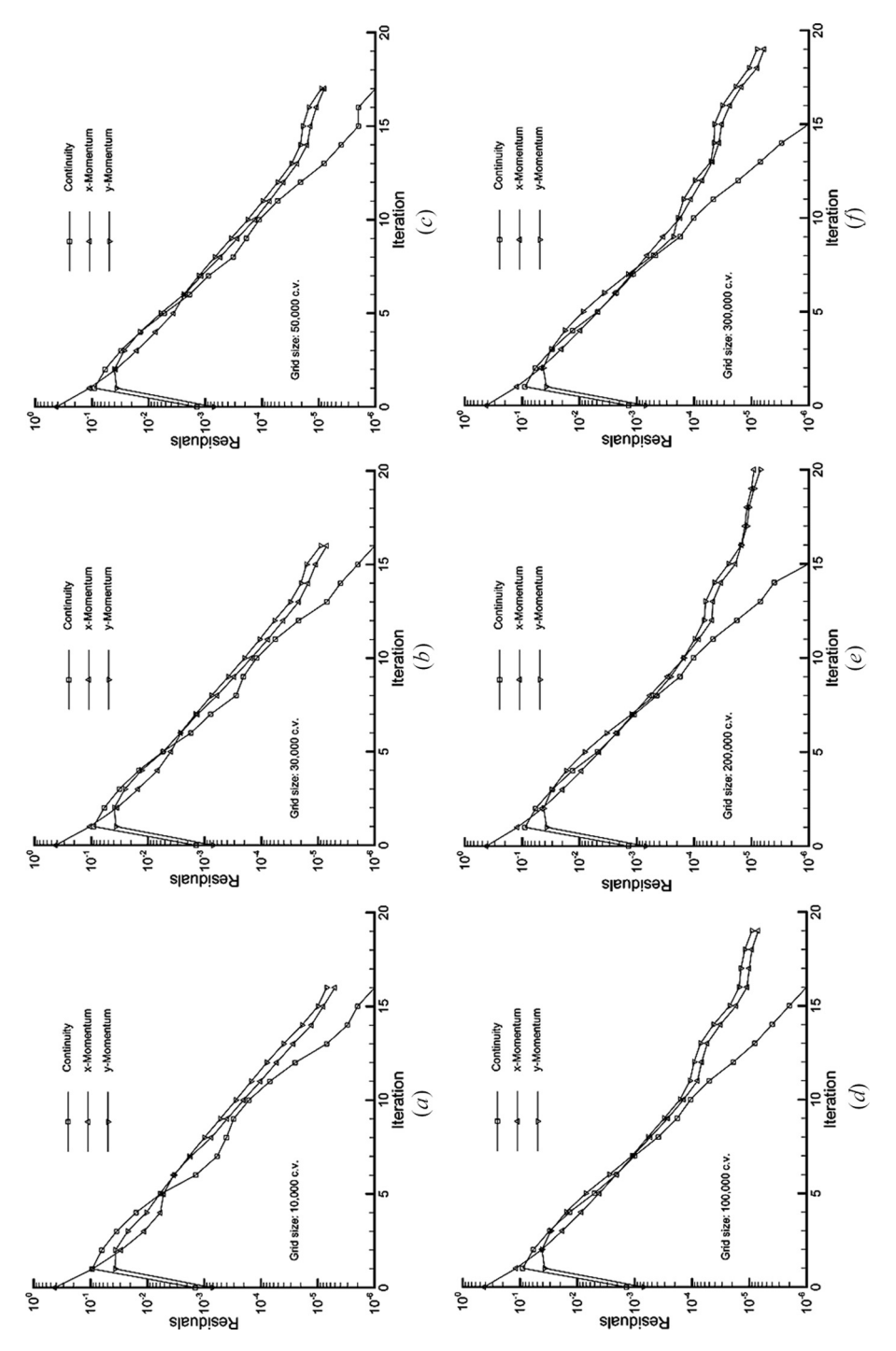


Figure 5. Residual history plots on the various grids for the lid-driven flow in a skew cavity.

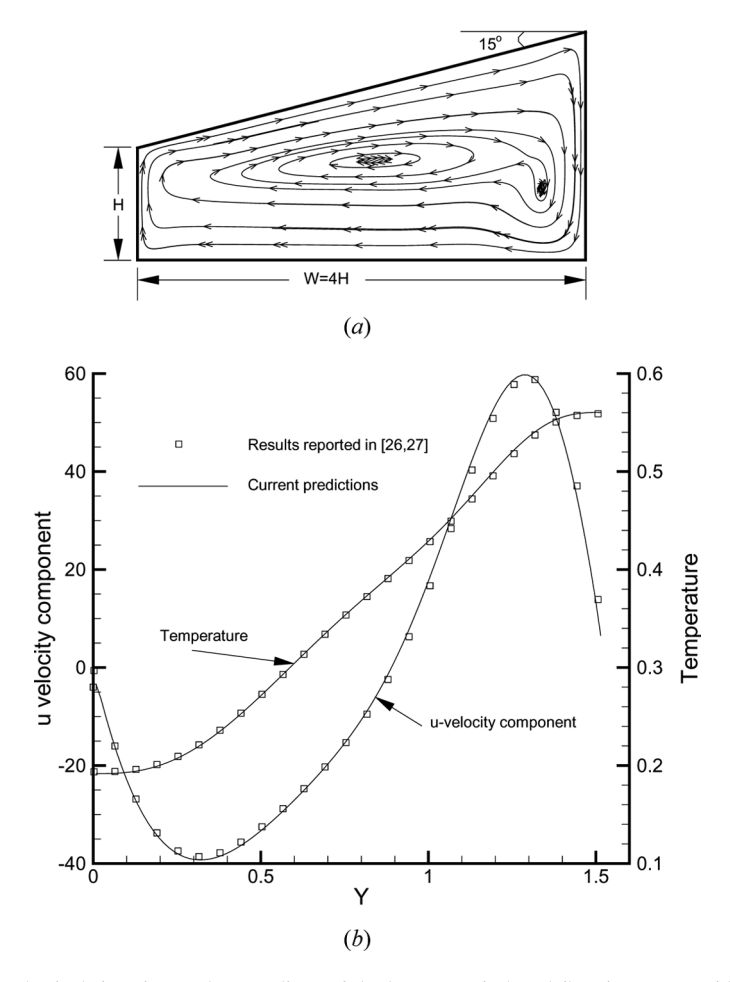


Figure 6. (a) Physical situation and streamlines of the buoyancy-induced flow in a trapezoidal cavity. (b) Comparison of predictions obtained with the newly coupled solver against results generated using a commercial code for the buoyancy-induced flow in a trapezoidal cavity.

Table 3. Number of iterations and computation time required by the coupled solver for the buoyancy-induced flow in a trapezoidal cavity

Size	Iterations	CPU (s)	CPU/CV (s)
10,000	25	44.42	0.00444
30,000	23	134.84	0.00449
50,000	22	233.92	0.00468
100,000	24	594.98	0.00595
200,000	23	1296.68	0.00648
300,000	22	2020.93	0.00674

CV, Control volume.

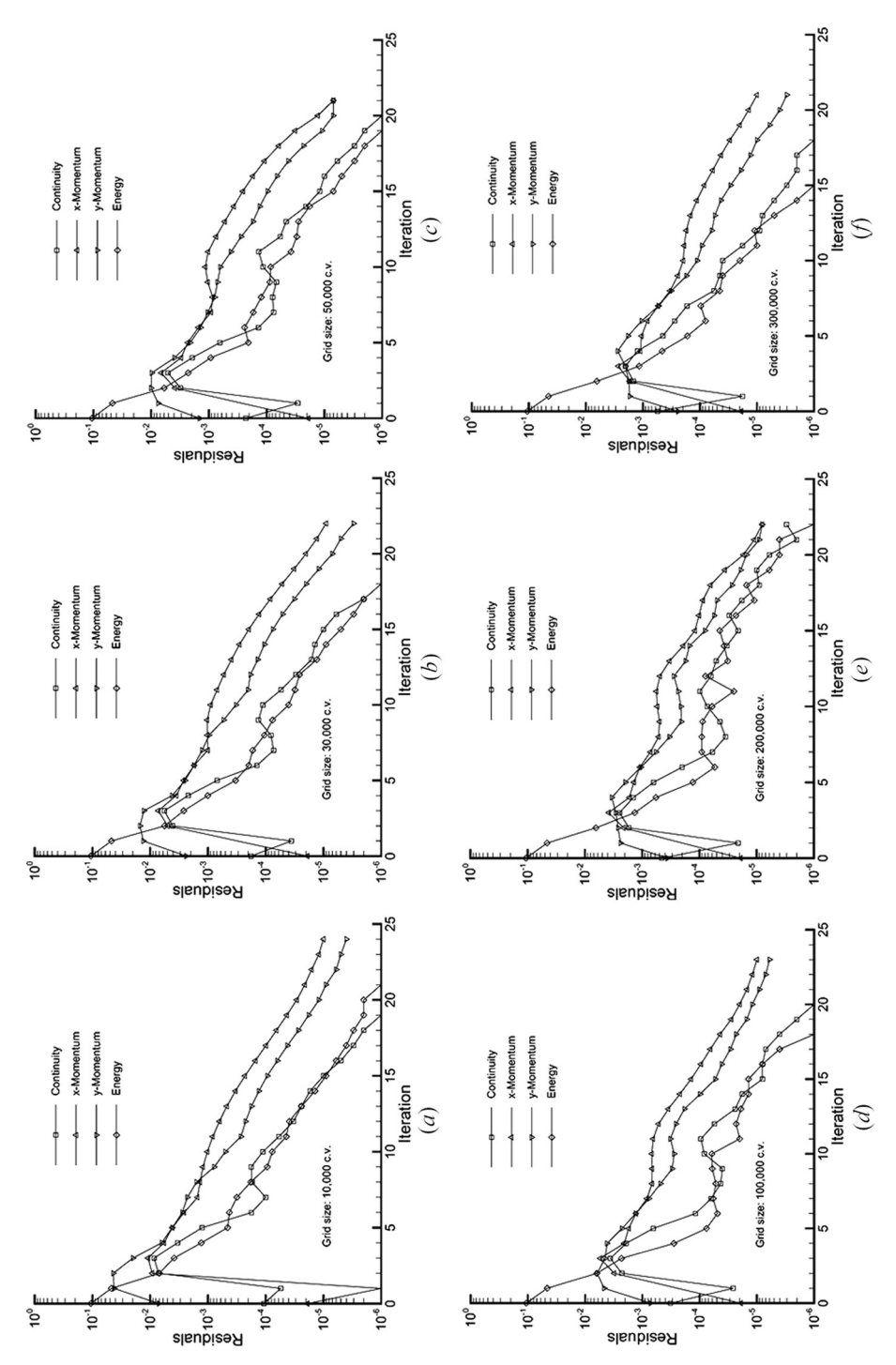


Figure 7. Residual history plots on the various grids for buoyancy-induced flow in a trapezoidal cavity.

CLOSING REMARKS

This article presented a fully coupled solver for the solution of laminar incompressible flows on structured collocate grids in which the pressure equation is derived in the same way as in the SIMPLE algorithm [1], yielding a set of diagonally dominant equations. The performance of the coupled algorithm was demonstrated by solving three laminar incompressible fluid flow problems: (1) flow behind a backward-facing step, (2) lid-driven flow in a skew cavity, and (3) natural convection in a trapezoidal cavity. Results showed that the CPU time per control volume is nearly independent of the grid size.

REFERENCES

- 1. S. V. Patankar and D. B. Spalding, A Calculation Procedure for Heat, Mass and Momentum Transfer in Three-Dimensional Parabolic Flows, *Int. J. Heat Mass Transfer*, vol. 15, pp. 1787–1806, 1972.
- 2. J. P. Van Doormaal and G. D. Raithby, Enhancement of the SIMPLE Method for Predicting Incompressible Fluid Flows, *Numer. Heat Transfer*, vol. 7, pp. 147–163, 1984.
- 3. S. V. Patankar, Numerical Heat Transfer and Fluid Flow, Hemisphere, New York, 1981.
- F. Moukalled and M. Darwish, A Unified Formulation of the Segregated Class of Algorithms for Fluid Flow at all Speeds, *Numer. Heat Transfer B*, vol. 37, pp. 103–139, 2000.
- 5. C. M. Rhie and W. L. Chow, A Numerical Study of the Turbulent Flow Past an Isolated Airfoil with Trailing Edge Separation, *AIAA J.*, vol. 21, pp. 1525–1532, 1983.
- C. Hsu, A Curvilinear-Coordinate Method for Momentum, Heat and Mass Transfer in Domains of Irregular Geometry, Ph.D. thesis, University of Minnesota, Minneapolis, MN, 1981.
- 7. W. Rodi, S. Majumdar, and B. Schonung, Finite Volume Methods for Two-Dimensional Incompressible Flows with Complex Boundaries, *Comput. Meth. Appl. Mech. Eng.*, vol. 75, pp. 369–392, 1989.
- 8. G. E. Schneider, G. D. Raithby, and M. M. Yonavovich, Finite Element Analysis of Incompressible Fluid Flow Incorporating Equal Order Pressure and Velocity Interpolation, in C. Taylor, K. Morgan, and C. A. Brebbia (eds.), *Numerical Methods in Laminar and Turbulent Flows*, pp. 89–102, Pentech Press, London, 1978.
- 9. L. S. Caretto, R. M. Curr, and D. B. Spalding, Two Numerical Methods for Three-Dimensional Boundary Layers, *Comput. Meth. Appl. Mech. Eng.*, vol. 1, pp. 39–57, 1972.
- 10. S. P. Vanka, Fully Coupled Calculation of Fluid Flows with Limited Use of Computer Storage, *Argonne Nat. Lab. Tech. Rep.*, pp. ANL-83–87, 1983.
- 11. K. C. Karki and H. C. Mongia, Evaluation of a Coupled Solution Approach for Fluid Flow Calculations in Body Fitted Coordinates, *Int. J. Numer. Meth. Fluids*, vol. 11, pp. 1–20, 1990.
- 12. M. E. Braaten, Development and Evaluation of Iterative and Direct Methods for the Solution of the Equations Governing Recirculating Flows, Ph.D. thesis, University of Minnesota, Minneapolis, MN, 1985.
- 13. Z. Mazhar, A Procedure for the Treatment of the Velocity–Pressure Coupling Problem in Incompressible Fluid Flow, *Numer. Heat Transfer B*, vol. 39, pp. 91–100, 2001.
- 14. R. F. Hanby and D. J. Silvester, A Comparison of Coupled and Segregated Iterative Solution Techniques for Incompressible Swirling Flow, *Int. J. Numer. Meth. Fluids*, vol. 22, pp. 353–373, 1996.

- 15. A. Pascau, C. Pérez, and F. J. Serón, A Comparison of Segregated and Coupled Methods for the Solution of the Incompressible Naveir-Stokes Equations, *Commun. Numer. Meth. Eng.*, vol. 12, pp. 617–630, 1996.
- 16. M. Zedan and G. E. Schneider, A Coupled Strong Implicit Procedure for Velocity and Pressure Computation in Fluid Flow Problems, *Numer. Heat Transfer*, vol. 8, pp. 537–558, 1985.
- 17. P. F. Galpin, J. P. Van Doormal, and G. D. Raithby, Solution of the Incompressible Mass and Momentum Equations by Application of a Coupled Equation Line Solver, *Int. J. Numer. Meth. Fluids*, vol. 5, pp. 615–625, 1985.
- 18. I. Ammara and C. Masson, Development of a Fully Coupled Control-Volume Finite Element Method for the Incompressible Naveir-Stokes Equations, *Int. J. Numer. Meth. Fluids*, vol. 44, pp. 621–644, 2004.
- J. P. Van Doormal, Numerical Methods for the Solution of Incompressible and Compressible Fluid Flows, Ph.D. thesis, University of Waterloo, Waterloo, Ontario, Canada, 1985.
- R. D. Lonsdale, An Algebraic Multigrid Scheme for Solving the Navier-Stokes Equations on Unstructured Meshes, *Proc. 7th Int. Conf. on Numerical Methods in Turbulent and Laminar Flows*, pp. 1432–1442, Stanford, CA, 1991.
- 21. R. Webster, An Algebraic Multigrid Solver for Navier-Stokes Problems, *Int. J. Numer. Meth. Fluids*, vol. 18, pp. 761–780, 1994.
- 22. R. Webster, An Algebraic Multigrid Solver for Navier-Stokes Problems in the Discrete Second-Order Approximation, *Int. J. Numer. Meth. Fluids*, vol. 22, pp. 1103–1123, 1996.
- M. Peric, R. Kessler, and G. Scheuerer, Comparison of Finite Volume Numerical Methods with Staggered and Collocated Grids, *Comput. Fluids*, vol. 16, pp. 289–403, 1988.
- S. K. Choi, H. Y. Nam, and M. Cho, A Calculation Procedure for Incompressible Flow in Complex Geometries Using Momentum Interpolation Method, *Proc. 7th Int. Conf. on Numerical Methods in Turbulent and Laminar Flows*, pp. 1634–1644, Stanford, CA, 1991.
- 25. F. Moukalled and M. Darwish, Natural Convection in a Trapezoidal Enclosure Heated from the Side with a Baffle Mounted on its Upper Inclined Surface, *Heat Transfer Eng.*, vol. 25, pp. 80–93, 2004.
- 26. F. Moukalled and M. Darwish, Natural Convection in a Partitioned Trapezoidal Cavity Heated from the Side, *Numer. Heat Transfer A*, vol. 43, pp. 543–563, 2003.